


Understanding Magnetic Resonance Imaging of Knee Cartilage Repair: A Focus on Clinical Relevance

CARTILAGE
2018, Vol. 9(3) 223–236
© The Author(s) 2017
Reprints and permissions:
sagepub.com/journalsPermissions.nav
DOI: 10.1177/1947603517710309
journals.sagepub.com/home/CAR


Daichi Hayashi^{1,2}, Xinning Li³, Akira M. Murakami¹,
Frank W. Roemer^{1,4}, Siegfried Trattnig⁵, and Ali Guermazi¹

Abstract

The aims of this review article are (a) to describe the principles of morphologic and compositional magnetic resonance imaging (MRI) techniques relevant for the imaging of knee cartilage repair surgery and their application to longitudinal studies and (b) to illustrate the clinical relevance of pre- and postsurgical MRI with correlation to intraoperative images. First, MRI sequences that can be applied for imaging of cartilage repair tissue in the knee are described, focusing on comparison of 2D and 3D fast spin echo and gradient recalled echo sequences. Imaging features of cartilage repair tissue are then discussed, including conventional (morphologic) MRI and compositional MRI techniques. More specifically, imaging techniques for specific cartilage repair surgery techniques as described above, as well as MRI-based semiquantitative scoring systems for the knee cartilage repair tissue—MR Observation of Cartilage Repair Tissue and Cartilage Repair OA Knee Score—are explained. Then, currently available surgical techniques are reviewed, including marrow stimulation, osteochondral autograft, osteochondral allograft, particulate cartilage allograft, autologous chondrocyte implantation, and others. Finally, ongoing research efforts and future direction of cartilage repair tissue imaging are discussed.

Keywords

articular cartilage, cartilage repair, knee, magnetic resonance imaging, radiology

Introduction

The first autologous chondrocyte transplantation surgery was described by Brittberg and colleagues in 1994.¹ Since then, knee cartilage repair or restoration surgery has evolved rapidly thanks to a number of factors including improvement of presurgical assessment, imaging techniques, increased availability of matrix products including both fresh and frozen allografts, and focused research on the clinical outcomes including all cartilage surgical techniques.² Cartilage repair or restoration surgery is aimed to alleviate patient symptoms, to promote cartilage healing, and to prevent or delay the onset of osteoarthritis. McAdams and colleagues published a review article on articular cartilage injuries in athletes and the available surgical repair technique in 2010.³ There are still a variety of barriers (including cost, regulatory, insurance, and logistical issues) between new cartilage repair products/techniques and their routine clinical applications.⁴ However over the past 7 years there have been significant advances in our scientific knowledge with regard to cartilage repair or restoration techniques and imaging methods for evaluating both preoperative defects and postoperative repair status. Our review article will describe the principles of morphologic and

compositional magnetic resonance imaging (MRI) techniques for the imaging of both cartilage repair and restoration surgery. We will then illustrate their application to longitudinal studies, and to illustrate the clinical relevance of pre- and postsurgical MRI with correlation to intraoperative images of various surgical techniques.

¹Quantitative Imaging Center, Department of Radiology, Boston University School of Medicine, Boston, MA, USA

²Department of Radiology, Yale New Haven Health at Bridgeport Hospital, Bridgeport, CT, USA

³Department of Orthopedic Surgery, Boston University School of Medicine, Boston, MA, USA

⁴Department of Radiology, University of Erlangen-Nuremberg, Erlangen, Germany

⁵Department of Biomedical Imaging and Image-Guided Therapy, Medical University of Vienna, Vienna, Austria

The work reported in this article was done at Boston University School of Medicine, Boston, MA, USA.

Corresponding Author:

Daichi Hayashi, Department of Radiology, Boston University School of Medicine, 820 Harrison Avenue, FGH Building 3rd Floor, Boston, MA 02118, USA.

Email: dhayashi@bu.edu

Imaging Features of Repair Tissue

Morphological Evaluation

Morphological MRI Techniques. MRI systems with high static magnetic fields can increase signal to noise ratio (SNR) and produce greater spatial resolution images than those with lower magnet strength, an important feature for cartilage imaging. Therefore, 1.5-Tesla (T) and 3-T magnet systems with extremity coils are recommended. In particular, the higher SNR allows isotropic 3D images to be acquired in a clinically relevant acquisition time. Advances in coil technology and parallel imaging techniques have also contributed to reduced scan times. The same acquisition techniques are used for repair tissue and native cartilage. High spatial resolution is essential to obtain images of diagnostic quality. In-plane resolution of 0.3 mm has been recommended to resolve fibrillation of the native cartilage surface using fat suppressed 3D gradient-recalled echo imaging.⁵ Similarly, fissures and incomplete cartilage repair tissue integration require high-resolution imaging. In this section, we describe the pulse sequences most commonly used for morphological assessment of cartilage and cartilage repair tissue.

Two-Dimensional (2D) Fast Spin Echo (FSE). Two-dimensional FSE or turbo spin echo imaging sequences provide excellent SNR, contrast between tissues, and faster acquisition times.⁶ 2D-FSE is the core imaging technique for the musculoskeletal system, in general, and the acquisition type most commonly used for clinical assessment of cartilage lesions; it is part of the cartilage imaging protocol recommended by International Cartilage Repair Society.⁷ The most common MRI acquisitions for morphological assessment of cartilage include proton density-weighted (PDW), intermediate-weighted (IW), and T2-weighted (T2W) sequences with or without fat suppression.⁸ On the other hand, T1W images are not considered to be cartilage-sensitive because they only allow poor differentiation between joint effusion and cartilage unless used in conjunction with MR arthrography. By comparison, fluid-sensitive images provide good evaluation of cartilage, ligaments, menisci, and edema-like marrow signal. T2W images provide greater contrast between cartilage surface and effusion and can detect subtle changes such as fibrillation, although the signal intensity (SI) in the cartilage near the osteochondral junction becomes low due to decreased signal intensity in the cartilage with longer TE times, which makes differentiation of the deeper layers of cartilage within the radial zone and at the tidemark challenging. PDW images (TE < 30 ms) provide good cartilage surface contrast and have shown high sensitivity for internal cartilage signal changes. IW imaging with longer echo times (TEs) (30-60 ms) combines the advantages of T2W and PDW imaging and is less prone to magic angle artifacts.⁹ Care should be taken to adjust the TE on each magnet

system to optimize visualization of the cartilage-fluid and cartilage-bone interfaces.

Three-Dimensional (3D) FSE. Two-dimensional FSE imaging often suffers from the need for thicker slices with resultant partial volume averaging effects that may be greater than in 3D acquisitions.⁸ To optimally view the cartilage and joint space, 2D-FSE also requires imaging acquisition in multiple planes, which is time consuming. Isotropic, or near isotropic, 3D sequences can produce higher spatial resolution and high-quality reformatted images in any plane. All image planes are potentially provided from a single sequence obviating the multiple acquisitions required to image all planes with standard 2D sequences. 3D-FSE acquisitions use an additional phase-encoding gradient for spatial encoding along the slice-select direction and generate a set of contiguous slices.¹⁰ The clinically available 3D-FSE sequences rely on flip-angle modulation to reduce blurring and parallel imaging to reduce scan time.⁸

Three-dimensional FSE sequences have a diagnostic accuracy similar or slightly inferior to 2D-FSE for evaluation of focal cartilage defects and other joint structures. It has been shown that 3D-FSE can be applied for multitissue assessment of the whole joint.¹¹⁻¹³ Additionally, IW 3D-FSE sequences with fat saturation allow for evaluation of subchondral bone, although image contrast is better with water sensitive 2D-FSE images.

Spoiled Gradient Recoiled Echo (SPGR). Fat suppression or water excitation 3D-SPGR, or similar fast low-angle shot (FLASH), imaging produces a contrast in which the SI of cartilage is greater than the surrounding tissues and joint fluid.⁸ However, unreliable image contrast between the cartilage and fluid or joint tissues may result in poor detection of subtle cartilage defects.¹⁴ An additional limitation is susceptibility artifacts, which can be prominent at some cartilage repair sites. Another problem with gradient recalled echo based (GRE) sequences, in general, is insensitivity to bone marrow edema and other joint pathology.^{15,16} While GRE sequences have been used for focal cartilage defect assessment,^{17,18} several recent studies have shown that they are less sensitive for focal defect detection than other techniques.^{16,19,20} These sequences are, however, excellent for cartilage segmentation and quantification of cartilage volume and thickness due to the good image contrast between cartilage and subchondral bone.^{21,22}

Dual-Echo Steady-State (DESS). DESS is another GRE imaging technique for cartilage that was introduced in the 1990s,²³ but did not become widely used until 3D-DESS could be performed with a short imaging time. Flip angles may be adjusted to optimize cartilage-fluid contrast to improve cartilage lesion detection.²⁴ Fat saturation or water excitation is typically used with DESS. The diagnostic

Table 1. Summary of MOCART Scoring System for Cartilage Repair Tissue.

| Features Evaluated | Scores |
|---|--|
| Defect fill (degree of defect repair and filling of the defect in relation to the adjacent cartilage) | 0%; 0% to 25%; 25% to 50%; 50% to 75%; 75% to 100%; 100%; 100% to 125%; 125% to 150%; 150% to 200%; >200% |
| Cartilage interface (integration with adjacent cartilage to border zone in two planes) | Scored using sagittal (femur, patella, trochlea, tibia), coronal (femur, tibia), and axial (patella, trochlea) planes. Complete; demarcating border visible (split-like); defect visible <50%; defect visible >50% |
| Bone interface (integration of the transplant to the subchondral bone; integration of a possible periosteal flap) | Complete; partial delamination; complete delamination; delamination |
| Surface (constitution of the surface of the repair tissue) | Surface intact; surface damaged <50% of depth; surface damaged >50% of depth; adhesions |
| Structure (constitution of the repair tissue) | Homogeneous; inhomogeneous or cleft formation |
| Signal intensity (intensity of MR signal in the repair tissue in comparison to the adjacent cartilage: normal = identical to adjacent cartilage; nearly normal = slight areas of signal alterations; abnormal = large areas of signal alteration) | Normal; nearly normal; abnormal |
| Subchondral lamina (constitution of the subchondral lamina) | Intact; not intact |
| Chondral osteophytes (osteophytes within the cartilage repair area) | Absent; osteophytes <50% of repair tissue; osteophytes >50% of repair tissue |
| Bone marrow edema (maximum size and localization in relation to the cartilage repair tissue and other alterations assessed in the 3D MOCART score) | Absent; small (<1 cm); medium (<2 cm); large (<4 cm); diffuse |
| Subchondral bone (constitution of the subchondral bone) | Intact; granulation tissue; cyst |
| Effusion (approximately size of joint effusion visualized in all planes) | Absent; small; medium; large |

performance of 3D-DESS for cartilage lesions is commensurate with 3D-GRE sequences.

Balanced Steady-State Free Precession (bSSFP). Three-dimensional bSSFP sequences provide excellent contrast between cartilage and adjacent synovial fluid with bright fluid SI compared to cartilage.²⁵ Magnetic field inhomogeneities may result in off-resonance artifacts worsened by long TRs. Short TRs can improve the images but result in longer acquisition times. The diagnostic accuracy of bSSFP for morphologic assessment of cartilage is similar to that of standard 2D- and 3D-GRE sequences.^{25,26} Fat suppression, water excitation, or a Dixon technique such as IDEAL are commonly used with bSSFP.²⁷ The use of combined IDEAL and bSSFP may result in higher SNR and cartilage-fluid contrast to noise ratio.²⁸

Semiquantitative Scoring

MRI Observation of Cartilage Repair Tissue (MOCART). MOCART is a reproducible semiquantitative scoring system for assessment of morphological cartilage repair. MOCART originally defined 9 structural variables but was modified to assess 11 variables, taking advantage of higher resolution 2D and isotropic 3D MR images, as summarized in **Table 1**.²⁹ This “3D-MOCART” improves evaluation by localizing the features within the repair site and the relation of the repair site to the weight-bearing regions of the joint,

evaluating the repair tissue-cartilage interfaces or “border zones,” in every plane, and providing a detailed subchondral bone assessment.²⁹ Since all of the original MOCART features are assessed by 3D-MOCART, for the sake of simplicity we will refer to both types as “MOCART.”²⁹ The usefulness of MOCART in a randomized controlled clinical trial of autologous cartilage tissue implants has been demonstrated in a study by Anderson and colleagues through its 5-year follow-up period.³⁰

When the repair tissue is as thick as the adjacent cartilage, defect fill is scored as 100%. Hypertrophy (>100%) and incomplete repair (<100%) are recorded in 25% increments. Kreuz *et al.* found that graft hypertrophy over 150% after autologous chondrocyte implantation (ACI) of full-thickness chondral defects in the knee usually required surgery while less severe hypertrophy could be watched.³¹

The cartilage-interface variable scores the integration of the repair to adjacent cartilage at the border zone. Absence of a gap between the repair tissue and native cartilage is considered “complete.” Incomplete integration is either a fissure-like border zone or a measurable defect and is scored as less than or more than 50% of the length of the defect in coronal, axial, and sagittal directions. Of note, the conspicuity of fissures at the area of integration with the host cartilage is a function of both the in-plane and through-plane resolutions.

The bone interface grades integration of the repair tissue to the subchondral bone. It is described as complete

Table 2. Summary of MRI Compositional Techniques.

| Compositional MRI Techniques | Cartilage Component Assessed | | | Advantages | Disadvantages |
|------------------------------|------------------------------|---------------|-----|--|--|
| | Collagen Network | Water Content | GAG | | |
| T2 mapping | Yes | Yes | No | No need for intravenous (IV) gadolinium; well validated; easy to implement | Long scan time using multiecho spin-echo sequence; cannot assess calcified cartilage at osteochondral junction |
| T2* mapping | Yes | Yes | No | No need for IV gadolinium; shorter scan time than T2 mapping; can be used with UTE to assess calcified cartilage at the osteochondral junction | Not well validated; susceptible to magnetic field inhomogeneities and magic angle effects |
| T1 rho imaging | No | Yes | Yes | No need for IV gadolinium; sensitive to early degeneration; may complement T2/T2* mapping | Nonspecific in terms of cartilage components assessed; limited availability; long scan time |
| Sodium imaging | No | No | Yes | No need for IV gadolinium; correlates directly with GAG content | Needs specialized hardware and coils; long scan time; low spatial resolution |
| dGEMRIC | No | No | Yes | Direct assessment of GAG content by inverse relation of GAG accumulation/contrast uptake; well validated | Needs IV gadolinium; 90 minutes delay between exercise and scanning |
| gagCEST | No | No | Yes | No need for IV gadolinium | Difficult to implement on clinical systems due to technical complexity; needs ultra-high field MRI; not well validated |
| Diffusion-weighted imaging | Yes | No | Yes | No need for IV gadolinium; provides additional information regarding cartilage microarchitecture | Semiquantitative image processing is demanding; susceptible to movement artifacts |
| Ultrashort TE imaging (UTE) | Yes | Yes | No | Can be used to assess tissue with intrinsic short T2 such as cartilage near osteochondral junction; can be used in conjunction with T2, T2* and T1 rho imaging | Limited availability |

References for **Table II.** ⁷⁰⁻⁷²

integration, partial delamination, or complete delamination. For periosteal ACI, partial or complete delamination of the periosteal flap is noted.

The repair tissue surface is considered “intact” when it is even and smooth, without evidence of damage or irregularity. When damage such as fibrillation or ulceration is present, it is scored as involving less than or more than 50% of the tissue thickness. Although rare, synovial adhesions attached to the repair tissue are recorded under the “surface” variable.

The repair tissue structure is classified as “homogenous” when a normal, layered cartilage appearance is seen over the entire repair site. If the structure is lost, it is classified as inhomogeneous. Additionally, if a cleft is present in the structure, it is mentioned specifically.

Based on the visual inspection of MR images, the SI of the repair tissue is considered normal if it is identical to the adjacent native cartilage. If the SI is hyper- or hypointense, it should be classified as “nearly normal” or “abnormal,” depending on the extent and/or degree of altered SI. This SI

variable is based on any cartilage-dedicated MR sequence; to simplify scoring, no specific acquisition type is specified.

The subchondral lamina, or bone plate, between the repair tissue and the bone marrow is classified as either intact or “not intact” if irregular.

Chondral osteophytes, that is, ossifications within the repair site above the level of the adjacent subchondral bone plate, are scored as absent or less than or more than 50% of the repair tissue thickness. Of note, chondral osteophytes are not uncommonly seen following the microfracture.

Bone marrow edema subjacent to the repair site is classified according to diameter as small (<1 cm), medium (<2 cm), large (<4 cm), or diffuse. The size of bone marrow edema is calculated in cm². If the edema is related to other pathology by MOCART scoring, this is noted.

MOCART also scores the subchondral bone marrow adjacent (beneath) to the repair site as intact if there is no abnormality, or note is made of granulation tissue, subchondral sclerosis, and cysts. Joint effusions are estimated by

visual inspection and graded as absent, small, moderate, or large.

Cartilage Repair Osteoarthritis Knee Score (CROAKS). MOCART is comprehensive for assessment of the repair site itself; however, assessment of the other structures of the joint is paramount to assess longitudinal outcomes and development of osteoarthritis. The CROAKS combines features of MOCART and the MRI osteoarthritis knee score,³² which is an established semiquantitative scoring system for whole organ assessment of the knee, to provide a comprehensive, reproducible tool for longitudinal postoperative assessment after surgical cartilage.³³

Table 2 shows the specific features outside of the repair site, assessed for multiple joint subregions by CROAKS. These include bone marrow lesions beyond the repair site, subchondral cysts, nonoperated cartilage status, osteophytes, synovitis, effusion, menisci, and anterior and posterior cruciate ligaments. Other periarticular features evaluated include the pes anserine bursa, iliotibial band, prepatellar bursa, infrapatellar bursa, and presence of popliteal cysts, ganglion cysts, and/or loose bodies.

Compositional MRI. At the molecular level, cartilage consists of approximately 70% to 80% fluid and 20% to 30% solid extracellular matrix (ECM).³⁴ The ECM is composed of a network of collagen fibrils and proteoglycan molecules; mostly aggrecans that consist of a protein core with covalently attached glycosaminoglycans (GAGs).^{34,35} GAGs are negatively charged and make up the majority of the “fixed charge density” of the ECM. Electroneutrality is maintained by the partitioning of cations, mainly sodium (Na^+), and anions, mainly chloride (Cl^-), between the cartilage and joint fluid. The biomechanical properties of cartilage are largely due to water flow within the ECM and the cartilage-joint fluid distribution of water that is, in part, dictated by the fixed charge density.

Compositional MRI acquisitions provide a way to detect biochemical and microstructural changes in the cartilage ECM even before gross morphological changes occur. Although not in routine clinical use, these techniques have been used extensively in cartilage research. Compositional MRI can supplement morphologic imaging, by potentially defining the biomechanical quality of cartilage repair tissue. The basic concepts of the compositional MRI techniques currently available to evaluate cartilage repair tissue are summarized in **Table 2**. Of note, the stratification of T2 relaxation times across the articular cartilage reflects changes in the orientation of collagen fibers in the extracellular matrix.³⁶ The disorganized tissue found in cartilage repair sites generally has greater water mobility and therefore more prolonged T2 relaxation times. Laminar analysis of normal articular hyaline cartilage T2 maps, that is, separate measurement of regions of interest of the superficial

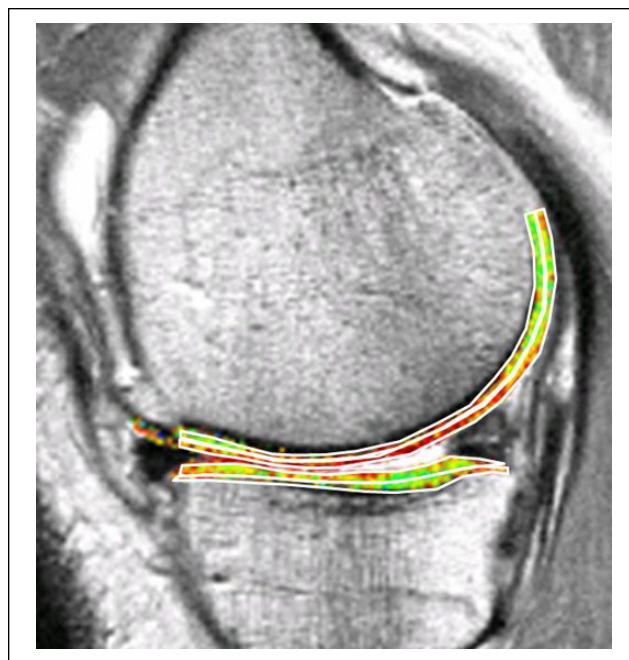


Figure 1. Bilaminar T2 relaxometry. Example of manual segmentation of the cartilage of the medial tibia and weight-bearing femoral condyle on a sagittal multi-echo spin echo (MESE) sequence. The tibial cartilage is segmented from its anterior to posterior end, and the femoral cartilage throughout a weight-bearing region of interest. As cartilage T2 is known to display spatial variation with tissue depth, the segmented cartilage plates subdivided into the top (superficial) and bottom (deep) 50%, based on the local distance between the segmented cartilage surface and bone interface. Color coding displays intrachondral variations in regional T2.

and deep halves of the cartilage (**Fig. 1**), has shown that T2 values are consistently higher at the articular level than at the bone interface. Restoration of a bilaminar structure with longer superficial T2 relaxation times in a cartilage repair site is indicative of maturation to a hyaline-like repair tissue.^{37,38} While there is more literature on compositional MRI of nonoperated, degenerating cartilage, a substantial amount of research has applied these methods for evaluation of cartilage repair tissue.³⁹

Currently Available Surgical Techniques

In this review, we will describe the following cartilage repair techniques: microfracture/marrow stimulation, osteochondral autograft/allograft (OATS) transplantation, particulate cartilage allograft, ACI, open reduction and internal fixation of a large osteochondral lesion, and femoral condyle transplantation. **Table 3** shows the summary of these techniques. Of note, a recent systematic review of randomized controlled trials of knee cartilage repair surgery concluded no single

Table 3. Overview of Cartilage Repair Techniques.

| Technique | Indications |
|--|---|
| Marrow stimulation/microfracture | Patients younger than 55 years; focal contained defect (surrounded by intact cartilage); no subchondral bone involvement; femoral condyles; smaller lesions of 2 cm ² or less have better outcome than larger lesions |
| Osteochondral autograft transplantation | Active patients younger than 50 years; smaller lesions of 2.5 cm ² or less; subchondral bone involvement; better rates of return to sports versus microfracture |
| Osteochondral allograft transplantation | Lesions with bone and cartilage loss; large, uncontained lesions (i.e., extending beyond the margin or the cartilage or deep into subchondral bone); lesions between 2 and 4 cm ² in diameter; particularly useful for revision of previously performed cartilage repair procedures, especially when the subchondral bone is damaged; needs fresh matched donor; expensive |
| Particulate cartilage allograft | Focal articular cartilage defects; contained lesions; lesions size <3 cm ² |
| Autologous chondrocyte transplantation | Large, full-thickness traumatic defects in patients between ages of 15 and 40 years; must have preserved subchondral bone with no involvement; requires two operations; outcome is mixed |
| Open reduction and internal fixation of a large osteochondral lesion (OCD) | Large traumatic defects or displaced OCD with preserved cartilage; acute injuries; fragment must be big enough to hold screws for fixation |
| Femoral condyle transplantation | Large area of avascular necrosis of the femur in younger patients; can be considered in extreme cases in young patients trying to avoid total knee replacement as a salvage procedure |

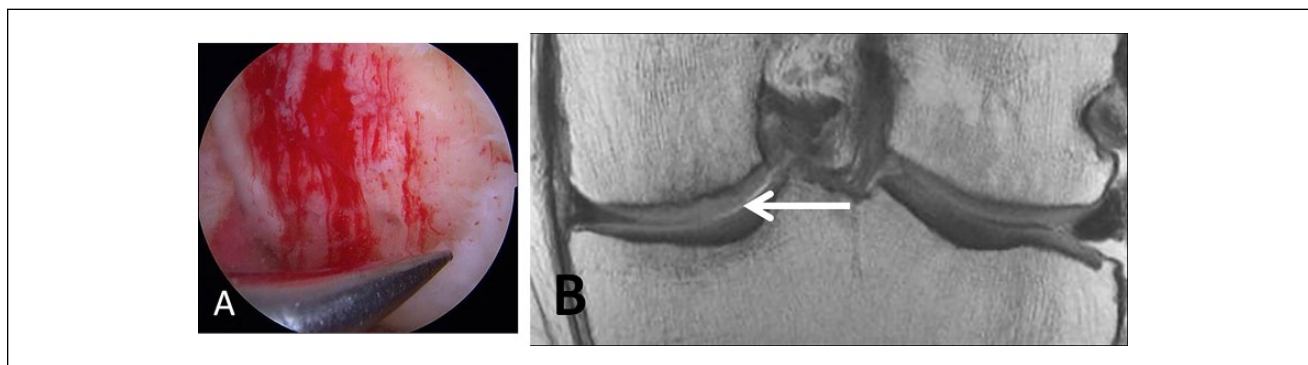


Figure 2. A 46-year-old male laborer who had surgical repair of a high-grade cartilage defect by a microfracture technique. **(A)** Microfracture or perforation of the subchondral bone. Note the filling of the defect with blood clot. **(B)** Coronal proton density-weighted TSE MRI at 10 months post microfracture treatment demonstrates new growth of fibrocartilaginous repair tissue over the defect.

treatment provides the single “best” clinical outcome among various available techniques.⁴⁰

Microfracture/Marrow Stimulation

The microfracture technique is the most commonly used procedure for the repair of focal cartilage defects.⁴¹ This procedure is aimed at inducing marrow stimulation, and it begins by the arthroscopic micropenetration of the cartilage defect surface to the subchondral bone until visible bleeding is achieved. Removal of calcified layer of cartilage is also performed. This allows mesenchymal stem cells from the subchondral bone marrow to be introduced into the debrided cartilage defect, which heal the defect by forming fibrocartilage tissue.⁴² This procedure is optimally indicated

in patients aged less than 40 years, with a focal contained cartilage defect that is surrounded by intact cartilage or with femoral condyle lesions and small defects <2 cm² (**Figs. 2 and 3**).⁴³⁻⁴⁵ Bone marrow stimulation techniques may be augmented with scaffolds or polymers (e.g., chitosan-based biomaterial, BST-CarGel), which stabilize the clot,⁴⁶ as well as bilayered synthetic plugs that promote gradient ingrowth of bone marrow cells into the porous scaffolds. The use of autologous platelet-rich plasma in association with the microfracture technique has been explored and seems to give better clinical and functional outcome in a short term compared to microfracture alone, but the clinical results of two groups were similar at 2 years.⁴⁷ Augmented microfracture with autogenous bone marrow concentrate was also shown to improve healing of repair site in the

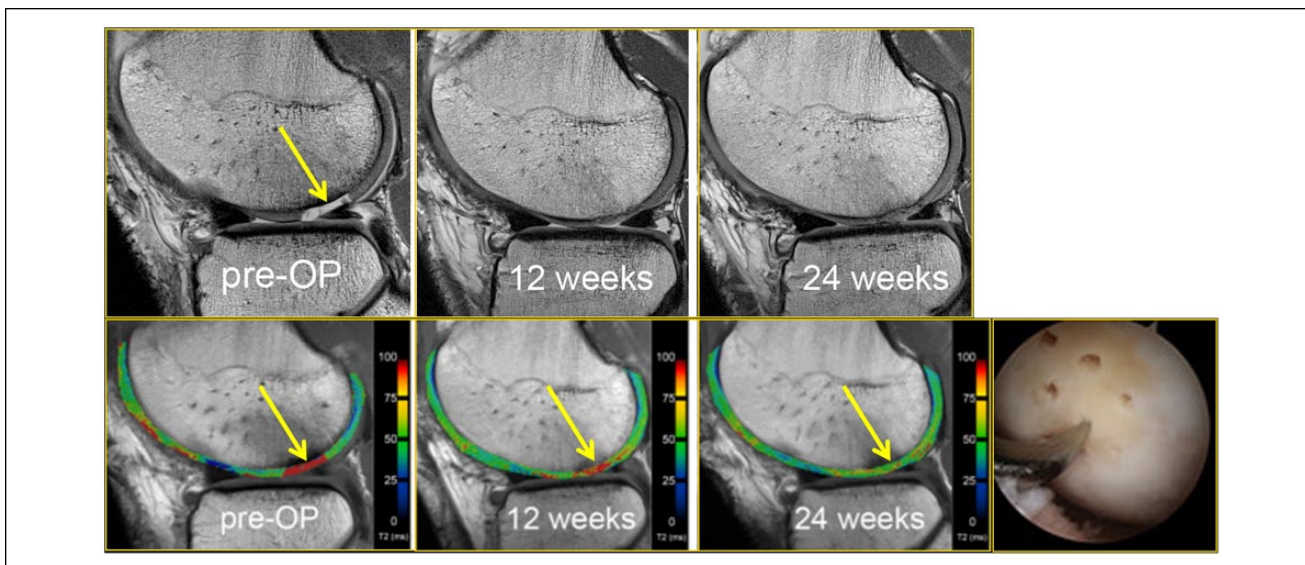


Figure 3. A 25-year-old male soccer player who received microfracture surgery of a cartilage lesion (yellow arrow, preoperative image). Arthroscopic image shows an arthroscopic awl at the site of lesion microfracture. Pre- and postoperative T2-mapping images show how T2 values change longitudinally, demonstrating the maturation of the repaired cartilage (yellow arrows, 6 weeks and 24 weeks postoperatively) with decreasing free water content and thus decreasing T2 values during the longitudinal follow-up. The patient returned to play 8 months after surgery.

equine model based on appropriate histology and illustrated by T2 mapping and T1 rho techniques.⁴⁸ Postoperatively, complete filling of the defect and differentiation of pluripotent stem cells into fibrocartilage can take several months to years. In the early postoperative period, the repair tissue appears hyperintense to native cartilage on T2W images, and the repair tissue may initially be indiscernible from fluid or appear very thin.⁴⁹ With repair tissue maturation, its signal intensity decreases and it may eventually appear hypointense to native cartilage.^{50,51} After 1 or 2 years, the repair tissue should have grown to fill the defect with a smooth and well-defined surface. Poorly filled defects and persistent underlying edema-like marrow signal intensity after 2 years may be indicative of incomplete peripheral integration of repair tissue.⁴⁹

Osteochondral Autograft Transplantation (OAT)

The OAT procedure begins by debriding damaged cartilage to create stable margins or cartilage borders around the defect. Donor osteochondral cylinders are harvested from non-weight-bearing margins of the trochlea either on the medial or lateral borders, near the intercondylar notch, or from other joints. Osteochondral grafts are then implanted into matching cylindrical recipient sites created at the cartilage defect (Fig. 4). OAT is optimally indicated in active patients aged 50 years or younger with small cartilage defects <2.5 cm² (Figs. 5 and 6).⁵² Outcome of OAT seems superior to the microfracture method in the young, active, and athletic patient population. A recent meta-analysis

showed OAT had a lower reoperation rate than microfracture at 5- and 10-year follow-up.⁵³

Application of a quantitative evaluation of articular surface curvature and 3D digital template for cartilage repair has been described and was shown to have a potential to optimize postsurgical restoration of joint articulation.⁵⁴ On early postoperative images, the graft should completely fill the defect with uniform signal intensity cartilage, without gaps between plugs and adjacent cartilage or adjacent bone. As bone incorporation progresses, the edema in the plugs and surrounding bone resolves and the plugs become indiscernible from the native tissue. Persistent edema-like marrow signal intensity within subchondral bone beyond 18 months and subchondral cyst formation may indicate poor tissue integration. Osteonecrosis is a rare complication of OATS.⁵⁵

Particulate Cartilage Allograft

Particulate cartilage allograft is a newer surgical technique for focal cartilage defects and comprises small approximately 1-mm cubes of particulated cartilage from a juvenile allograft donor (age <13 years) (Fig. 5).⁵⁶ The graft is applied to cartilage defects in a monolayer and held in place with the use of fibrin sealant during a single-step procedure.⁵⁶ Transplanted particulated cartilage cells are thought to escape from the extracellular matrix and migrate, multiply, and form a new hyaline-like cartilage tissue matrix that integrates with the surrounding recipient tissue. Feasibility, safety, and efficacy of this technique have been

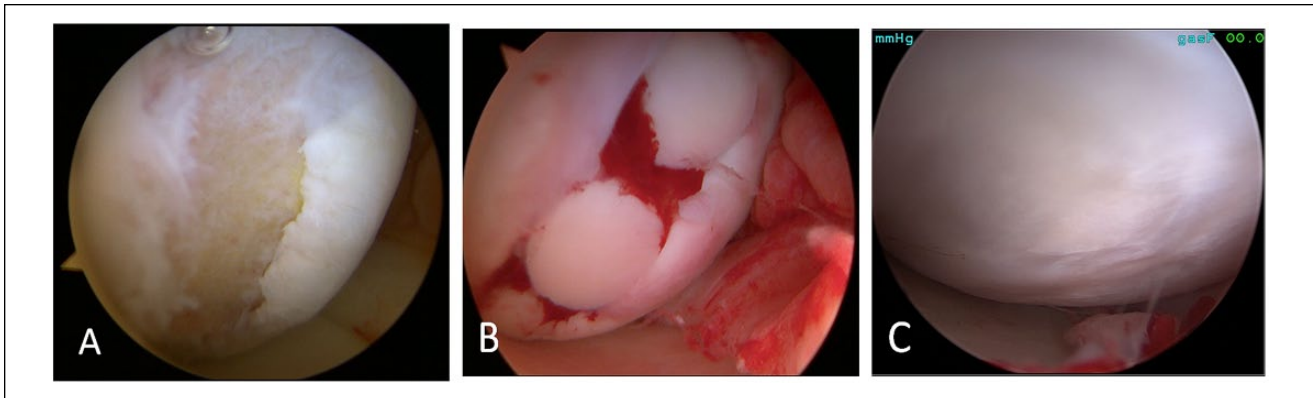


Figure 4. A 21-year-old mixed martial arts fighter who sustained a full-thickness cartilage defect, anterior cruciate ligament tear, and meniscal tears and who had repair of an osteochondral lesion of the medial femoral condyle by osteochondral autograft transfer system (OATS). **(A)** Arthroscopy image shows full thickness cartilage defects with involvement of the subchondral bone after debridement in the femoral condyle. Three 6-mm plugs donor osteochondral cylinders were harvested from non-weight bearing margins of the medial and lateral trochlea ridge. **(B)** Open medial knee arthrotomy status post osteochondral autologous transplantation with the three plugs. **(C)** A second look arthroscopy 1 year after the surgery shows complete healing of the entire surgical site after OATS procedure.

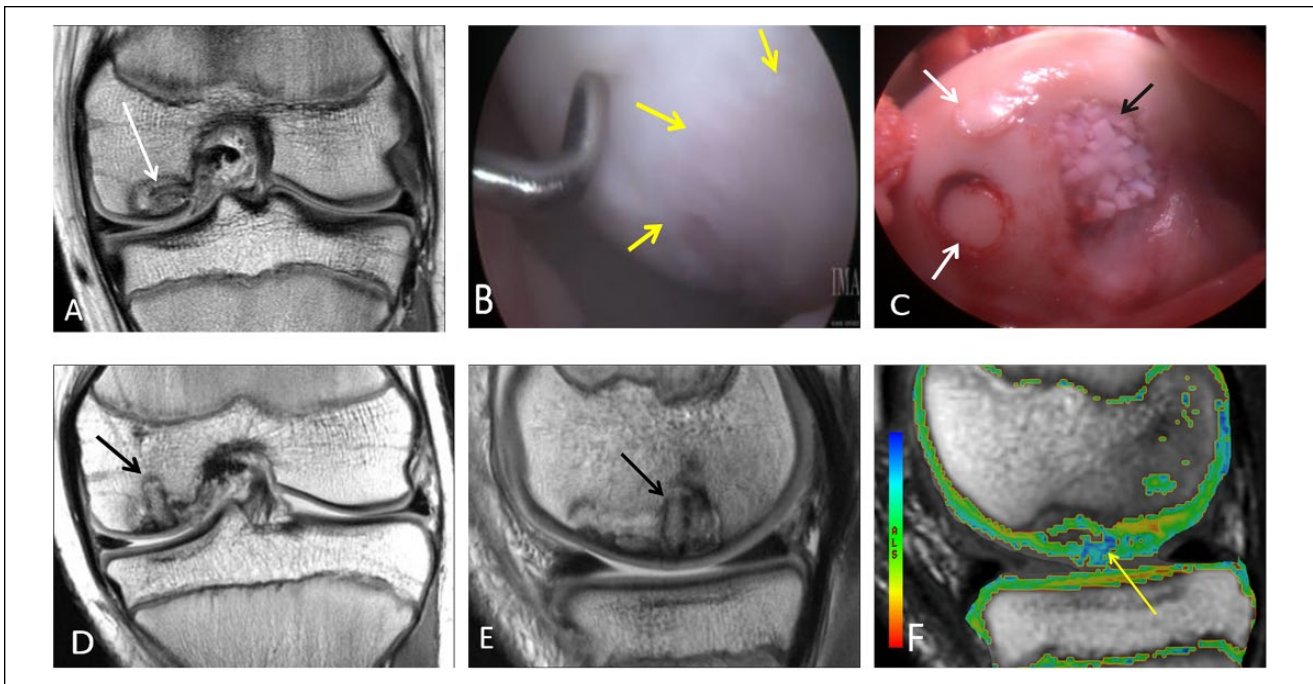


Figure 5. An 11-year-old male who had repair of an osteochondral lesion by osteochondral autograft transfer system (OATS) and de novo juvenile cartilage transplantation technique. Coronal **(A)** proton density-weighted TSE MRI shows a large unstable osteochondral lesion over the medial femoral condyle. **(B)** Arthroscopy view of the lesion over the central weight bearing surface of the medial femoral condyle. The arrows are outlining the edge of the osteochondral lesion. **(C)** Two OATS autografts placed in situ into the osteochondral lesion (white arrows). De novo particulate juvenile cartilage transplantation onto the medial femoral condyle lesion is seen (black arrow). Coronal **(D)** and sagittal **(E)** proton density-weighted TSE MRI 2 months later demonstrate partial bony incorporation of the osteochondral plug (black arrows). Note the presence of residual osteochondral lesion that is not covered by the single plug approach, closer to the intercondylar notch. This is noted lateral to the lesion in the coronal image **(D)** and anterior to the lesion in sagittal image **(E)**. T2 mapping MRI **(F)** shows residual increased T2 relaxation values (yellow arrow) at the margins of the osteochondral transfer. Two years postoperatively, the patient is pain-free and returned to playing sports.

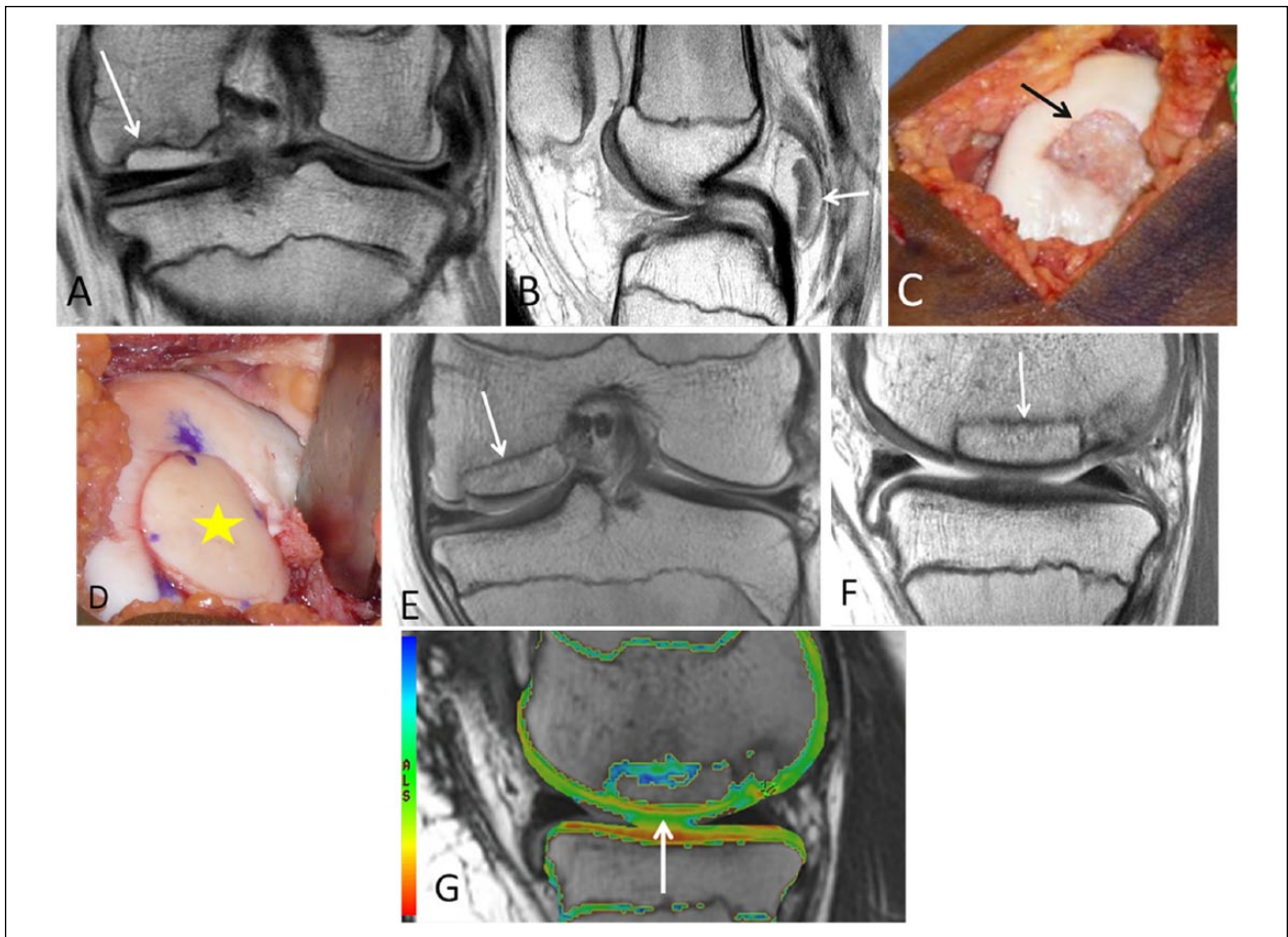


Figure 6. A 15-year-old male who had cartilage repair with osteochondral allograft transplantation and osteochondral autograft transfer system (OATS) for an osteochondral lesion. Coronal (**A**) and sagittal (**B**) proton density-weighted TSE MRI demonstrate a large osteochondral defect over the medial femoral condyle with partial collapse of the subchondral plate (**A**, arrow). The osteochondral fragment is displaced posterior to the posterior cruciate ligament (**B**, arrow). (**C**) Operative view of the large osteochondral lesion, noting the partial collapse (arrow) of the articular surface seen on MRI. (**D**) Placement of an osteochondral allograft matched from a fresh cadaver donor (yellow star) and an osteochondral autograft plug, harvested from the patient's medial trochlea. (**E**, **F**, **G**) Coronal (**E**) and sagittal (**F**) proton density-weighted TSE MRI 2 months later demonstrate partial bony incorporation of the osteochondral allograft transplant and autograft plug. T2 mapping MRI (**G**) shows T2 relaxation values over the grafts that are similar to the native undamaged cartilage. Note is made of the lack of hyaline orientation at the area of peripheral integration, likely reflecting the characteristic fissures of fibrocartilage at the area of peripheral integration with the host tissue.

demonstrated in short-term studies with up to 2 years of follow-up, but long-term evidence from randomized controlled trials is still lacking.^{57,58} Postoperative MRI may demonstrate persistent subchondral edema and nonuniform chondral surface after several months to 2 years.⁵⁹

Osteochondral Allograft Transplantation

The osteochondral allograft technique involves harvesting cartilage and bone from a fresh cadaveric donor. Allografts are not limited by the amount of donor tissue, and thus cartilage defects >3 cm² in diameter can be repaired (**Fig. 6**). Because the entire cartilage-bone unit is transplanted with osteochondral allografts,

they can be particularly useful for revision of previously performed and failed cartilage repair procedures, especially when the subchondral bone is damaged. This procedure is optimally indicated for large uncontained chondral defects with bone and cartilage loss (i.e., extend beyond the margin of cartilage or deep into subchondral bone).^{60,61} A recent systematic review demonstrated osteochondral allografts can improve clinical outcome scores with good durability at a high rate of successful outcome (75%) at 12.3 years after surgery.⁶²

MRI assessment of osteochondral allografts includes evaluation of graft signal intensity, defect fill, cartilage edge integration at host-graft junction, articular surface congruity, subchondral bone plate congruity and bone marrow

signal, osseous integration, and presence of cystic changes of graft.⁶³ Initial defect fill is expected with a smooth articular contour. Diffuse bone marrow edema is expected during the first 3 months postoperatively. With progressive bone incorporation, an advancing high-signal-intensity front develops. Graft marrow signal intensity eventually normalizes. Edema-like marrow signal intensity persisting for more than 12 months or articular surface collapse may be indicative of eventual failure of treatment. MRI features suggestive of delayed or poor allograft incorporation include the presence of persistent fluid signal intensity within the graft, discernible fissure (cartilage edge integration) or cleft (osseous integration) at host-graft junction, disrupted subchondral bone plate integrity, and presence of cystic changes of graft at host-graft junction.^{63,64} Additionally, MRI may help detect potential host-immune response to the allograft tissue, which is demonstrated on MRI as abnormal host marrow edema, thick host-graft interface, and abnormal graft marrow signal intensity.⁶⁵

Autologous Chondrocyte Implantation

This two-part procedure begins by arthroscopic harvesting of chondrocytes, usually from the cartilage on the tibial spines.¹ They are subsequently cultured and multiplied *ex vivo* for 6 to 8 weeks, and then implanted into the chondral defect together with fibrin glue to fix the edges (**Fig. 7**). This technique is optimally indicated for large lesions $>2\text{ cm}^2$. ACI has been shown to result in satisfactory clinical outcome with improved knee function, pain and mental health for adolescent patients over a long-term follow-up (mean 9.6 years).⁶⁶

Postoperatively, complete integration of the graft is demonstrated on MRI by the presence of complete filling of the chondral defect with the repair tissue to the expected level of adjacent cartilage.⁴⁹ Underfilling of the repair site signifies incomplete defect fill. Incomplete integration of repair tissue after ACI is termed “delamination,” which can be identified by displacement of all or a portion of the graft from the repair site or linear fluid intensity between the repair tissue and underlying bone.⁴⁹ A common complication after ACI is periosteal cover hypertrophy, which is depicted on MRI as a graft being thicker than the native cartilage with resultant distortion of articular contour. Adhesions are another postoperative complication commonly seen in the peripatellar regions. Poor integration of the ACI with the subchondral bone is indicated by persistent or increasing edema-like signal in the marrow beneath an ACI site.⁴⁹

Other Techniques

Open reduction and internal fixation (ORIF) is indicated for large traumatic defects or displaced osteochondral lesions (**Fig. 8**). These lesions are typically unstable with edema or fluid deep to the osteochondral lesion that is detectable on

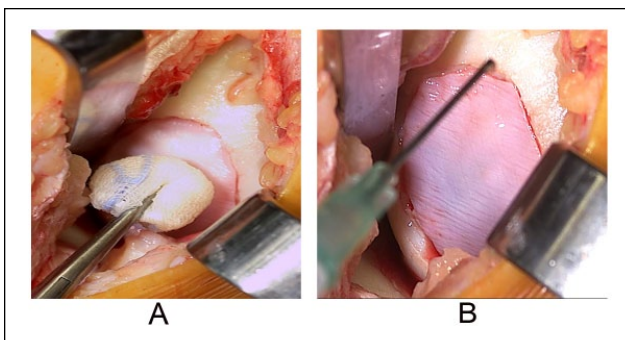


Figure 7. Example of autologous chondrocyte implantation procedure for a femoral cartilage defect $>2\text{ cm}$, showing the second step of the procedure, that is, implantation of chondrocytes (**A**) followed by covering of the implantation site with a synthetic collagen membrane (**B**), which is sutured to the cartilage edges over the defect and made watertight.

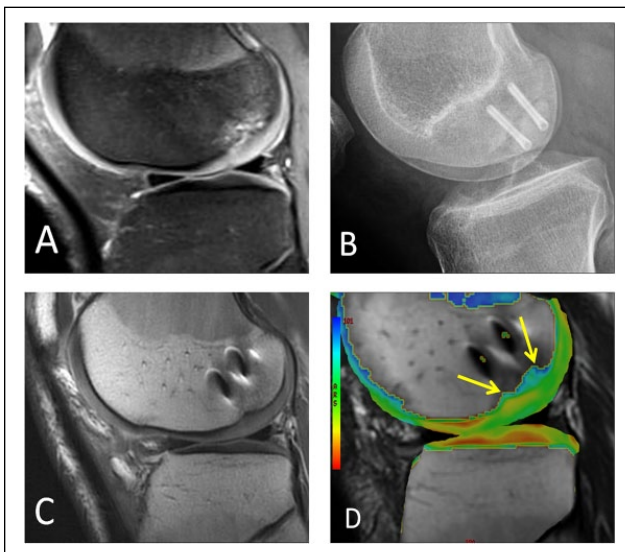


Figure 8. A different male patient who underwent open reduction and internal fixation of a large osteochondral lesion. (**A**) Large loose OCD lesion is seen on sagittal fat-suppressed proton density-weighted MRI in the lateral femoral condyle. (**B**) Postoperative lateral radiograph shows two metallic screws fusing the OCD lesion. (**C**) Postoperative sagittal proton density-weighted MRI shows integration of the fused OCD lesion with susceptibility artifact from screws. (**D**) Postoperative sagittal T2 mapping MRI shows prolongation of relaxation times with a lack of hyaline orientation over the central weight-bearing surface of the condyle over the lesion (arrows).

MRI. This surgical technique can be applied to both skeletally mature and immature patients.^{67,68} Headless metal compression screws provide a satisfactory union rate for the treatment of unstable OCD lesions of the femoral condyles at mean postoperative follow-up period of 31 months.⁶⁷ Some authors advocate the use of bioabsorbable fixation for symptomatic stable lesions in skeletally immature patients.⁶⁸

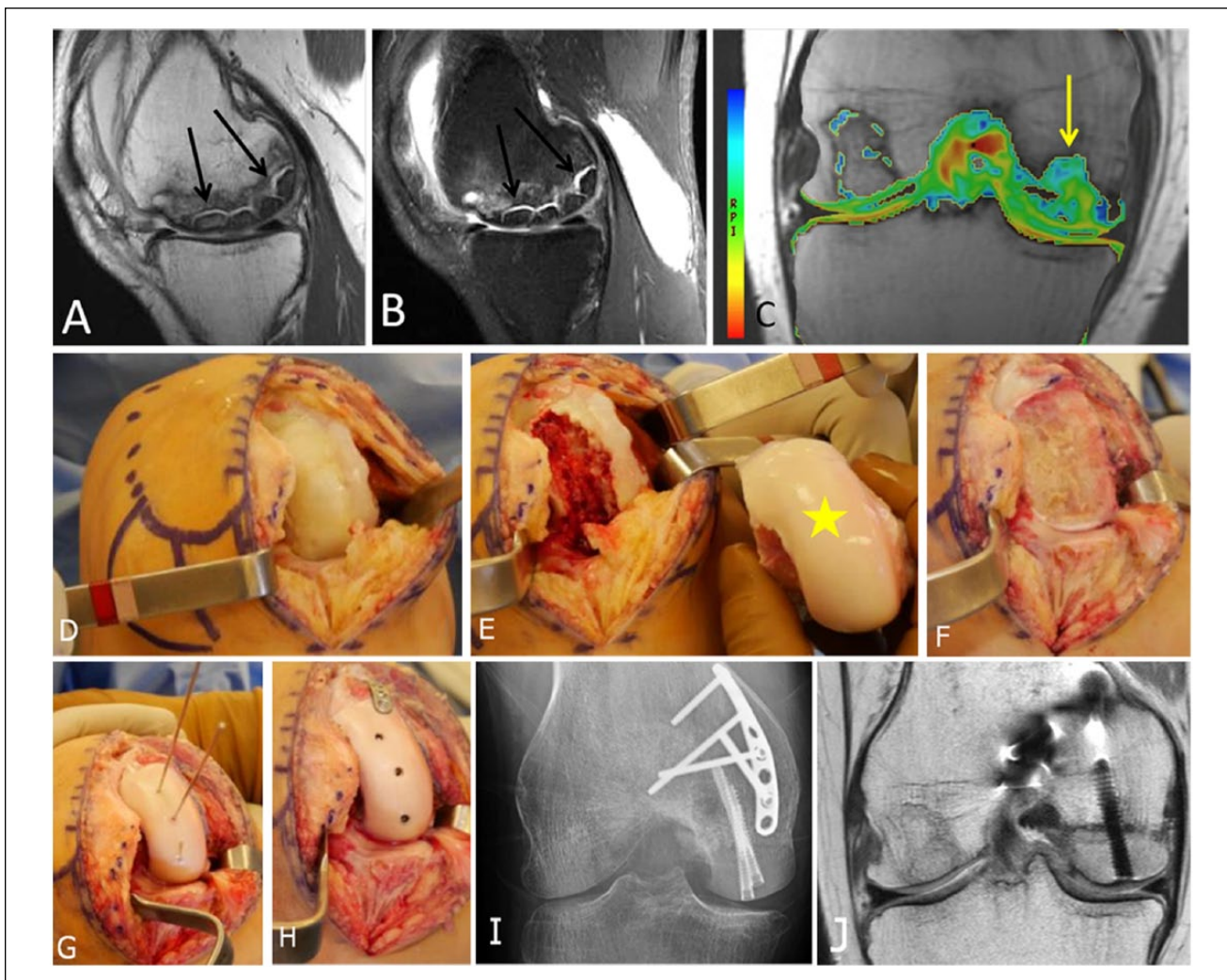


Figure 9. A 26-year-old female who had medial femoral condyle transplantation with matched fresh allograft. (**A, B**) Large areas of avascular necrosis is seen in both the sagittal (**A**) T1- and (**B**) fat-suppressed T2-weighted MRI (arrows). (**C**) Coronal T2 mapping MRI also shows prolongation of tissue relaxation times in the cartilage over the area of transplanted medial femoral condyle (arrow) compared to the lateral condyle. (**D**) Open arthrotomy of the knee is performed and the AVN of the medial femoral condyle is seen. The large area of AVN is debrided and seen in **E**. The matched femoral condyle is seen holding up to the defect (yellow star). (**F**) Free cut of the medial femoral condyle is performed. (**G**) The matched condyle is shaped to match the defect. Three wires are used to hold the condyle to the defect. (**H**) Three headless screws are inserted along with a small anti-shear plate to hold and fix the condyle transplantation. (**I, J**) Six months postoperative AP radiograph (**I**) and coronal proton density-weighted MRI (**J**) show metallic plate and screws transfixing the medial femoral condyle transplant in place, with evidence of successful incorporation and healing.

For postoperative imaging after ORIF using metallic hardware, susceptibility artifact can cause image degradation. Such artifact can be reduced by various strategies such as the use of a wide receiver bandwidth, view angle tilting (VAT) pulse, and ultimately 3D multispectral imaging techniques such as slice encoding for metal artifact reduction (SEMAC) or multiacquisition variable resonance image combination (MAVRIC).⁶⁹

Femoral condyle transplant can be performed for large areas of avascular necrosis with associated osteochondral lesions of the femur in young patients who are not candidates

of a unilateral knee replacement (**Fig. 9**). However, clinical efficacy and long-term outcomes of this technique as a method for cartilage repair has not been well established in the literature due to the complexity and rarity of the surgery.

Conclusion

All cartilage repair techniques have the same primary goal: to decrease pain symptoms, to improve mobility and function, and to prevent the progression of osteoarthritis. The various cartilage repair surgery techniques discussed have shown to

improve functional outcomes; however, assessing the efficacy within the orthopedic literature is limited by heterogeneity in surgical technique, lesion type, patient characteristics, and reporting of nonstandardized outcome measures. There is urgent need to define outcomes clinically and by MRI measurements including local assessment and with regard to long-term osteoarthritis development/progression. In clinical practice, the MRI assessment of repair tissue relies heavily on morphologic imaging. The main role of MRI during the pre-surgery assessment is to give a detailed description of the defect size, depth of the lesion, and associated subchondral bony changes in order to help determining the best treatment choice. Compositional MRI provides the opportunity to measure the biochemical and microstructural time-dependent processes of maturation occurring within the repair tissue. Compositional MRI techniques are mostly used in research and for clinical trials, but they hold great promise for the clinical determination of surgical success. Before they can become clinically useful, however, compositional MRI techniques must be standardized and validated for cartilage repair tissue assessment and made time efficient. The combination of MRI-based morphologic and compositional imaging plays an integral role in the assessment of cartilage repair tissue and its integration to native tissues after cartilage repair surgery.

Acknowledgment and Funding

The author(s) received no financial support for the research, authorship, and/or publication of this article.

Declaration of Conflicting Interests

The author(s) declared the following potential conflicts of interest with respect to the research, authorship, and/or publication of this article: Ali Guermazi is the President of Boston Imaging Core Lab (BICL), LLC, and a consultant for Merck Serono, Genzyme, GE Healthcare, Pfizer, TissueGene, Ortho Trophix, and Astra Zeneca. Frank W. Roemer is a shareholder of BICL. Xinning Li is a Consultant for Tornier Shoulder Arthroplasty and Depuy Mitek Sports Medicine. The other authors have no conflicts of interest to disclose.

References

1. Brittberg M, Lindahl A, Nilsson A, Ohlsson C, Isaksson O, Peterson L. Treatment of deep cartilage defects in the knee with autologous chondrocyte transplantation. *N Engl J Med*. 1994;331:889-95.
2. Richter DL, Schenck RC Jr, Wascher DC, Treme G. Knee articular cartilage repair and restoration techniques: a review of the literature. *Sports Health*. 2016;8:153-60.
3. McAdams TR, Mithoefer K, Scopp JM, Mandelbaum BR. Articular cartilage injury in athletes. *Cartilage*. 2010;1:165-79.
4. Farr J, Gomoll AH. 2016 barriers to cartilage restoration. *J Clin Orthop Trauma*. 2016;7:183-6.
5. Rubenstein JD, Li JG, Majumdar S, Henkelman RM. Image resolution and signal-to-noise ratio requirements for MR imaging of degenerative cartilage. *AJR Am J Roentgenol*. 1997;169:1089-96.
6. Kijowski R, Blankenbaker DG, Davis KW, Shinki K, Kaplan LD, De Smet AA. Comparison of 1.5- and 3.0-T MR imaging for evaluating the articular cartilage of the knee joint. *Radiology*. 2009;250:839-48.
7. Bobic V; ICRS Articular Cartilage Imaging Committee. ICRS MR imaging protocol for knee articular cartilage. Wetzikon, Switzerland: International Cartilage Repair Society; 2000. p. 12.
8. Crema MD, Roemer FW, Marra MD, Burstein D, Gold GE, Eckstein F, *et al*. Articular cartilage in the knee: current MR imaging techniques and applications in clinical practice and research. *Radiographics*. 2011;31:37-61.
9. Zhuo J, Gullapalli RP. AAPM/RSNA physics tutorial for residents: MR artifacts, safety, and quality control. *Radiographics*. 2006;26:275-97.
10. Mugler JP 3rd. Optimized three-dimensional fast-spin-echo MRI. *J Magn Reson Imaging*. 2014;39:745-67.
11. Kijowski R, Davis KW, Woods MA, Lindstrom MJ, De Smet AA, Gold GE, *et al*. Knee joint: comprehensive assessment with 3D isotropic resolution fast spin-echo MR imaging—diagnostic performance compared with that of conventional MR imaging at 3.0 T. *Radiology*. 2009;252:486-95.
12. Crema MD, Nogueira-Barbosa MH, Roemer FW, Marra MD, Niu J, Chagas-Neto FA, *et al*. Three-dimensional turbo spin-echo magnetic resonance imaging (MRI) and semi-quantitative assessment of knee osteoarthritis: comparison with two-dimensional routine MRI. *Osteoarthritis Cartilage*. 2013;21:428-33.
13. Subhas N, Kao A, Freire M, Polster JM, Obuchowski NA, Winalski CS. MRI of the knee ligaments and menisci: comparison of isotropic-resolution 3D and conventional 2D fast spin-echo sequences at 3 T. *AJR Am J Roentgenol*. 2011;197:442-50.
14. Yoshioka H, Stevens K, Genovese M, Dillingham MF, Lang P. Articular cartilage of knee: normal patterns at MR imaging that mimic disease in healthy subjects and patients with osteoarthritis. *Radiology*. 2004;231:31-8.
15. Crema MD, Roemer FW, Hayashi D, Guermazi A. Comment on: Bone marrow lesions in people with knee osteoarthritis predict progression of disease and joint replacement: a longitudinal study. *Rheumatology (Oxford)*. 2011;50:996-7.
16. Hayashi D, Guermazi A, Kwok CK, Hannon MJ, Moore C, Jakicic JM, *et al*. Semiquantitative assessment of subchondral bone marrow edema-like lesions and subchondral cysts of the knee at 3T MRI: a comparison between intermediate-weighted fat-suppressed spin echo and dual echo steady state sequences. *BMC Musculoskelet Disord*. 2011;12:198.
17. Disler DG, McCauley TR, Kelman CG, Fuchs MD, Ratner LM, Wirth CR, *et al*. Fat-suppressed three-dimensional spoiled gradient-echo MR imaging of hyaline cartilage defects in the knee: comparison with standard MR imaging and arthroscopy. *AJR Am J Roentgenol*. 1996;167:127-32.
18. Disler DG, McCauley TR, Wirth CR, Fuchs MD. Detection of knee hyaline cartilage defects using fat-suppressed three-dimensional spoiled gradient-echo MR imaging: comparison with standard MR imaging and correlation with arthroscopy. *AJR Am J Roentgenol*. 1995;165:377-82.

19. Roemer FW, Kwok CK, Hannon MJ, Crema MD, Moore CE, Jakicic JM, *et al.* Semiquantitative assessment of focal cartilage damage at 3T MRI: a comparative study of dual echo at steady state (DESS) and intermediate-weighted (IW) fat suppressed fast spin echo sequences. *Eur J Radiol.* 2011;80:e126-31.
20. Mohr A. The value of water-excitation 3D FLASH and fat-saturated PDw TSE MR imaging for detecting and grading articular cartilage lesions of the knee. *Skeletal Radiol.* 2003;32:396-402.
21. Eckstein F, Sittek H, Milz S, Putz R, Reiser M. The morphology of articular cartilage assessed by magnetic resonance imaging (MRI). Reproducibility and anatomical correlation. *Surg Radiol Anat.* 1994;16:429-38.
22. Ding C, Cicuttini F, Scott F, Cooley H, Boon C, Jones G. Natural history of knee cartilage defects and factors affecting change. *Arch Intern Med.* 2006;166:651-8.
23. Hardy PA, Recht MP, Piraino D, Thomasson D. Optimization of a dual echo in the steady state (DESS) free-precession sequence for imaging cartilage. *J Magn Reson Imaging.* 1996;6:329-35.
24. Moriya S, Miki Y, Yokobayashi T, Ishikawa M. Three-dimensional double-echo steady-state (3D-DESS) magnetic resonance imaging of the knee: contrast optimization by adjusting flip angle. *Acta Radiol.* 2009;50:507-11.
25. Duc SR, Pfirrmann CW, Schmid MR, Zanetti M, Koch PP, Kalberer F, *et al.* Articular cartilage defects detected with 3D water-excitation true FISP: prospective comparison with sequences commonly used for knee imaging. *Radiology.* 2007;245:216-23.
26. Duc SR, Koch P, Schmid MR, Horger W, Hodler J, Pfirrmann CW. Diagnosis of articular cartilage abnormalities of the knee: prospective clinical evaluation of a 3D water-excitation true FISP sequence. *Radiology.* 2007;243:475-82.
27. Gerdes CM, Kijowski R, Reeder SB. IDEAL imaging of the musculoskeletal system: robust water fat separation for uniform fat suppression, marrow evaluation, and cartilage imaging. *AJR Am J Roentgenol.* 2007;189:W284-91.
28. Gold GE, Hargreaves BA, Vasanawala SS, Webb JD, Shimakawa AS, Brittain JH, *et al.* Articular cartilage of the knee: evaluation with fluctuating equilibrium MR imaging—initial experience in healthy volunteers. *Radiology.* 2006;238:712-8.
29. Welsch GH, Zak L, Mamisch TC, Paul D, Lauer L, Mauerer A, *et al.* Advanced morphological 3D magnetic resonance observation of cartilage repair tissue (MOCART) scoring using a new isotropic 3D proton-density, turbo spin echo sequence with variable flip angle distribution (PD-SPACE) compared to an isotropic 3D steady-state free precession sequence (True-FISP) and standard 2D sequences. *J Magn Reson Imaging.* 2011;33:180-8.
30. Anderson DE, Williams RJ 3rd, DeBerardino TM, Taylor DC, Ma CB, Kane MS, *et al.* Magnetic resonance imaging characterization and clinical outcomes after NeoCart surgical therapy as a primary reparative treatment for knee cartilage injuries. *Am J Sports Med.* 2017;45(4):875-83.
31. Kreuz PC, Steinwachs M, Erggelet C, Krause SJ, Ossendorf C, Maier D, *et al.* Classification of graft hypertrophy after autologous chondrocyte implantation of full-thickness chondral defects in the knee. *Osteoarthritis Cartilage.* 2007;15:1339-47.
32. Hunter DJ, Guermazi A, Lo GH, Grainger AJ, Conaghan PG, Boudreau RM, *et al.* Evolution of semi-quantitative whole joint assessment of knee OA: MOAKS (MRI Osteoarthritis Knee Score). *Osteoarthritis Cartilage.* 2011;19:990-1002.
33. Roemer FW, Guermazi A, Trattinig S, Apprich S, Marlovits S, Niu J, *et al.* Whole joint MRI assessment of surgical cartilage repair of the knee: Cartilage Repair OsteoArthritis Knee Score (CROAKS). *Osteoarthritis Cartilage.* 2014;22:779-99.
34. Binks DA, Hodgson RJ, Ries ME, Foster RJ, Smye SW, McGonagle D, *et al.* Quantitative parametric MRI of articular cartilage: a review of progress and open challenges. *Br J Radiol.* 2013;86:20120163.
35. Buckwalter JA, Mankin HJ. Articular cartilage: degeneration and osteoarthritis, repair, regeneration, and transplantation. *Instr Course Lect.* 1998;47:487-504.
36. Potter HG, Foo LF. Magnetic resonance imaging of articular cartilage: trauma, degeneration, and repair. *Am J Sports Med.* 2006;34:661-77.
37. Welsch GH, Mamisch TC, Domayer SE, Dorotka R, Kutschal-Lissberg F, Marlovits S, *et al.* Cartilage T2 assessment at 3-T MR imaging: in vivo differentiation of normal hyaline cartilage from reparative tissue after two cartilage repair procedures—initial experience. *Radiology.* 2008;247:154-61.
38. Welsch GH, Mamisch TC, Marlovits S, Glaser C, Friedrich K, Hennig FF, *et al.* Quantitative T2 mapping during follow-up after matrix-associated autologous chondrocyte transplantation (MACT): full thickness and zonal evaluation to visualize the maturation of cartilage repair tissue. *J Orthop Res.* 2009;27:957-63.
39. Guermazi A, Roemer FW, Alizai H, Winalski CS, Welsch G, Brittberg M, *et al.* State of the art: MR imaging after knee cartilage repair surgery. *Radiology.* 2015;277:23-43.
40. Devitt BM, Bell SW, Webster KE, Feller JA, Whitehead TS. Surgical treatments of cartilage defects of the knee: systematic review of randomized controlled trials. *Knee.* Epub Feb 8, 2017. doi:10.1016/j.knee.2016.12.002.
41. McCormick F, Harris JD, Abrams GD, Frank R, Gupta A, Hussey K, *et al.* Trends in the surgical treatment of articular cartilage lesions in the United States: an analysis of a large private-payer database over a period of 8 years. *Arthroscopy.* 2014;30:222-6.
42. Mithoefer K, Williams RJ, Warren RF, Potter HG, Spock CR, Jones EC, *et al.* Chondral resurfacing of articular cartilage defects in the knee with the microfracture technique. *Surgical technique.* *J Bone Joint Surg Am.* 2006;88(Suppl 1, Pt 2):294-304.
43. Mithoefer K. Complex articular cartilage restoration. *Sports Med Arthrosc Rev.* 2013;21:31-7.
44. Mithoefer K, McAdams T, Williams RJ, Kreuz PC, Mandelbaum BR. Clinical efficacy of the microfracture technique for articular cartilage repair in the knee: an evidence-based systematic analysis. *Am J Sports Med.* 2009;37:2053-63.
45. Mundi R, Bedi A, Chow L, Crouch S, Simunovic N, Sibilsky Enselman E, *et al.* Cartilage restoration of the knee: a systematic review and meta-analysis of level 1 studies. *Am J Sports Med.* 2016;44:1888-95.
46. Steinwachs MR, Waibl B, Mumme M. Arthroscopic treatment of cartilage lesions with microfracture and BST-CarGel. *Arthrosc Tech.* 2014;3:e399-402.

47. Mancò A, Goderecci R, Rughetti A, De Giorgi S, Necozone S, Bernardi A, *et al.* Microfracture versus microfracture and platelet-rich plasma: arthroscopic treatment of knee chondral lesions. A two-year follow-up study. *Joints*. 2016;4:142-7.
48. Fortier LA, Potter HG, Rickey EJ, Schnabel LV, Foo LF, Chong LR, *et al.* Concentrated bone marrow aspirate improves full-thickness cartilage repair compared with microfracture in the equine model. *J Bone Joint Surg Am*. 2010;92:1927-37.
49. Alparslan L, Winalski CS, Boutin RD, Minas T. Postoperative magnetic resonance imaging of articular cartilage repair. *Semin Musculoskelet Radiol*. 2001;5:345-63.
50. Mithoefer K, Williams RJ 3rd, Warren RF, Potter HG, Spock CR, Jones EC, *et al.* The microfracture technique for the treatment of articular cartilage lesions in the knee: a prospective cohort study. *J Bone Joint Surg Am*. 2005;87:1911-20.
51. Choi YS, Potter HG, Chun TJ. MR imaging of cartilage repair in the knee and ankle. *Radiographics*. 2008;28:1043-59.
52. Farr J, Cole B, Dhawan A, Kercher J, Sherman S. Clinical cartilage restoration: evolution and overview. *Clin Orthop Relat Res*. 2011;469:2696-705.
53. Riboh JC, Cvetanovich GL, Cole BJ, Yanke AB. Comparative efficacy of cartilage repair procedures in the knee: a network meta-analysis. *Knee Surg Sports Traumatol Arthrosc*. Epub Sep 7, 2016. doi:10.1007/s00167-016-4300-1.
54. Barber L, Koff MF, Virtue P, Lipman JP, Hotchkiss RJ, Potter HG. The use of MRI modeling to enhance osteochondral transfer in segmental Kienbock's disease. *Cartilage*. 2012;3:188-93.
55. Link TM, Mischung J, Wörtler K, Burkart A, Rummeny EJ, Imhoff AB. Normal and pathological MR findings in osteochondral autografts with longitudinal follow-up. *Eur Radiol*. 2006;16:88-96.
56. Farr J, Cole BJ, Sherman S, Karas V. Particulated articular cartilage: CAIS and De Novo NT. *J Knee Surg*. 2012;25:23-29.
57. Farr J, Tabet SK, Margerrison E, Cole BJ. Clinical, radiographic, and histological outcomes after cartilage repair with particulated juvenile articular cartilage: a 2-year prospective study. *Am J Sports Med*. 2014;42:1417-25.
58. Tompkins M, Hamann JC, Diduch DR, Bonner KF, Hart JM, Gwathmay FW, *et al.* Preliminary results of a novel single-stage cartilage restoration technique: particulated juvenile articular cartilage allograft for chondral defects of the patella. *Arthroscopy*. 2013;29:1661-70.
59. Saltzman BM, Lin J, Lee S. Particulated juvenile articular cartilage allograft transplantation for osteochondral talar lesions. *Cartilage*. 2017;8:61-72.
60. Gortz S, Bugbee WD. Fresh osteochondral allografts: graft processing and clinical applications. *J Knee Surg*. 2006;19:231-40.
61. Demange M, Gornoll AH. The use of osteochondral allografts in the management of cartilage defects. *Curr Rev Musculoskelet Med*. 2012;5:1053-9.
62. Assenmacher AT, Pareek A, Reardon PJ, Macalena JA, Stuart MJ, Krych AJ. Long-term outcomes after osteochondral allograft: a systematic review at long-term follow-up of 12.3 years. *Arthroscopy*. 2016;32:2160-8.
63. Chang EY, Pallante-Kichura AL, Bae WC, Du J, Statum S, Wolfson T, *et al.* Development of a comprehensive osteochondral allograft MRI scoring system (OCAMRISS) with histopathologic, micro-computed tomography, and biomechanical validation. *Cartilage*. 2014;5:16-27.
64. Williams RJ 3rd, Ranawat AS, Potter HG, Carter T, Warren RF. Fresh stored allografts for the treatment of osteochondral defects of the knee. *J Bone Joint Surg Am*. 2007;89:718-26.
65. Sirlin CB, Brossmann J, Boutin RD, Pathria MN, Convery FR, Bugbee W, *et al.* Shell osteochondral allografts of the knee: comparison of MR imaging findings and immunologic responses. *Radiology*. 2001;219:35-43.
66. Ogura T, Bryant T, Minas T. Long-term outcomes of autologous chondrocyte implantation in adolescent patients. *Am J Sports Med*. 2017;45(5):1066-74.
67. Barrett I, King AH, Riester S, van Wijnen A, Levy BA, Stuart MJ, *et al.* Internal fixation of unstable osteochondritis dissecans in the skeletally mature knee with metal screws. *Cartilage*. 2016;7:157-62.
68. Webb JE, Lewallen LW, Christophersen C, Krych AJ, McIntosh AL. Clinical outcome of internal fixation of unstable juvenile osteochondritis dissecans lesions of the knee. *Orthopedics*. 2013;36:e1444-9.
69. Filli L, Jud L, Luechinger R, Nanz D, Andreisek G, Runge VM, *et al.* Material-dependent implant artifact reduction using SEMAC-VAT and MAVRIC: a prospective MRI phantom study. *Invest Radiol*. 2017;52(6):381-7.
70. Guermazi A, Alizai H, Crema MD, Trattinig S, Regatte RR, Roemer FW. Compositional MRI techniques for evaluation of cartilage degeneration in osteoarthritis. *Osteoarthritis Cartilage*. 2015;23:1639-53.
71. Bae WC, Biswas R, Chen K, Chang EY, Chung CB. UTE MRI of the osteochondral junction. *Curr Radiol Rep*. 2014;2:35.
72. Chang EY, Du J, Chung CB. UTE imaging in the musculoskeletal system. *J Magn Reson Imaging*. 2015;41:870-83.